

See discussions, stats, and author profiles for this publication at: <https://www.researchgate.net/publication/235739209>

# Nanomechanical Properties of Proteins and Membranes Depend on Loading Rate and Electrostatic Interactions

ARTICLE in ACS NANO · MARCH 2013

Impact Factor: 12.88 · DOI: 10.1021/nn400015z · Source: PubMed

---

CITATIONS

16

---

READS

46

## 2 AUTHORS:



Izhar Medalsy

Bruker Corporation

14 PUBLICATIONS 234 CITATIONS

[SEE PROFILE](#)



Daniel J Müller

ETH Zurich

255 PUBLICATIONS 12,914 CITATIONS

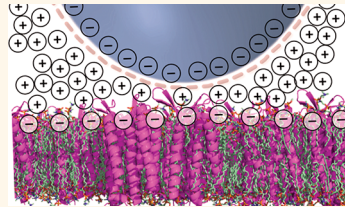
[SEE PROFILE](#)

# Nanomechanical Properties of Proteins and Membranes Depend on Loading Rate and Electrostatic Interactions

Izhar D. Medalsy<sup>‡</sup> and Daniel J. Müller<sup>‡,\*</sup>

<sup>‡</sup>Department of Biosystems Science and Engineering, ETH Zurich, CH-4058 Basel, Switzerland

**ABSTRACT** Knowing the dynamic mechanical response of tissue, cells, membranes, proteins, nucleic acids, and carbohydrates to external perturbations is important to understand various biological and biotechnological problems. Atomic force microscopy (AFM)-based approaches are the most frequently used nanotechnologies to determine the mechanical properties of biological samples that range in size from microscopic to (sub)nanoscopic. However, the dynamic nature of biomechanical properties has barely been addressed by AFM imaging. In this work, we characterize the viscoelastic properties of the native light-driven proton pump bacteriorhodopsin of the purple membrane of *Halobacterium salinarum*. Using force–distance curve (*F*–*D*)-based AFM we imaged purple membranes while force probing their mechanical response over a wide range of loading rates (from ~0.5 to 100  $\mu$ N/s). Our results show that the mechanical stiffness of protein and membrane increases with the loading rate up to a factor of 10 (from ~0.3 to 3.2 N/m). In addition, the electrostatic repulsion between AFM tip and sample can alter the mechanical stiffness measured by AFM up to ~60% (from ~0.8 to 1.3 N/m). These findings indicate that the mechanical response of membranes and proteins and probably of other biomolecular systems should be determined at different loading rates to fully understand their properties.



**KEYWORDS:** AFM · atomic force microscopy · bacteriorhodopsin · electrostatic double layer · lipid membrane · loading rate · mechanical stiffness · membrane protein · purple membrane · rheology

The combination of nanoscopic imaging and mechanical characterization of biological systems became possible with the invention of atomic force microscopy (AFM).<sup>1–5</sup> So far the mechanical properties of many biological systems ranging from organisms, tissues, cells, membranes, viruses, proteins, nucleic acids, and other macromolecular structures have been investigated by AFM.<sup>6–14</sup> Most biological systems show heterogeneous mechanical properties at the molecular scale. These heterogeneous mechanical properties are ultimately linked to biological function.<sup>15–18</sup> Thus, it is of advantage to record the mechanical properties of a biological sample at a spatial resolution sufficiently high to observe this heterogeneity. In the so-called force–volume (FV)-AFM mode the AFM contours the biological sample surface and pixel for pixel approaches AFM tip and sample to record a force–distance (*F*–*D*) curve. These *F*–*D* curves map the mechanical properties of the sample to the sample topography. Because FV-AFM is a brand name of an AFM company and the same or similar AFM mode can also

be operated by AFMs from other companies one may use a neutral definition such as *F*–*D* curve-based AFM. However, for many years FV-AFM was suffering from technical limitations such as slow imaging speed, limited number of pixels, poor force resolution (*ca.* 0.1–1 nN), and poor spatial resolution (*ca.* 10–50 nm).<sup>2</sup> Recent developments have pushed the limits of FV-AFM to detect biological forces in the pN regime,<sup>19</sup> at a spatial resolution approaching 1 nm,<sup>20–22</sup> and at scanning times approaching that of conventional AFMs (~8 min/image). Because of this development FV-AFM is increasingly used to characterize the mechanical properties of biological (and other) samples. However, in most applications of FV-AFM a fundamental consideration, the loading rate, is neglected. Single-molecule force spectroscopy (SMFS) teaches us that mechanical properties of molecular bonds, such as those formed between ligands and receptors, or bonds stabilizing proteins or DNA, are loading-rate dependent.<sup>23–27</sup> This loading rate describes the force applied to stress a bond within a certain time.

\* Address correspondence to daniel.mueller@bsse.ethz.ch.

Received for review January 2, 2013  
and accepted February 26, 2013.

Published online February 26, 2013  
10.1021/nn400015z

© 2013 American Chemical Society

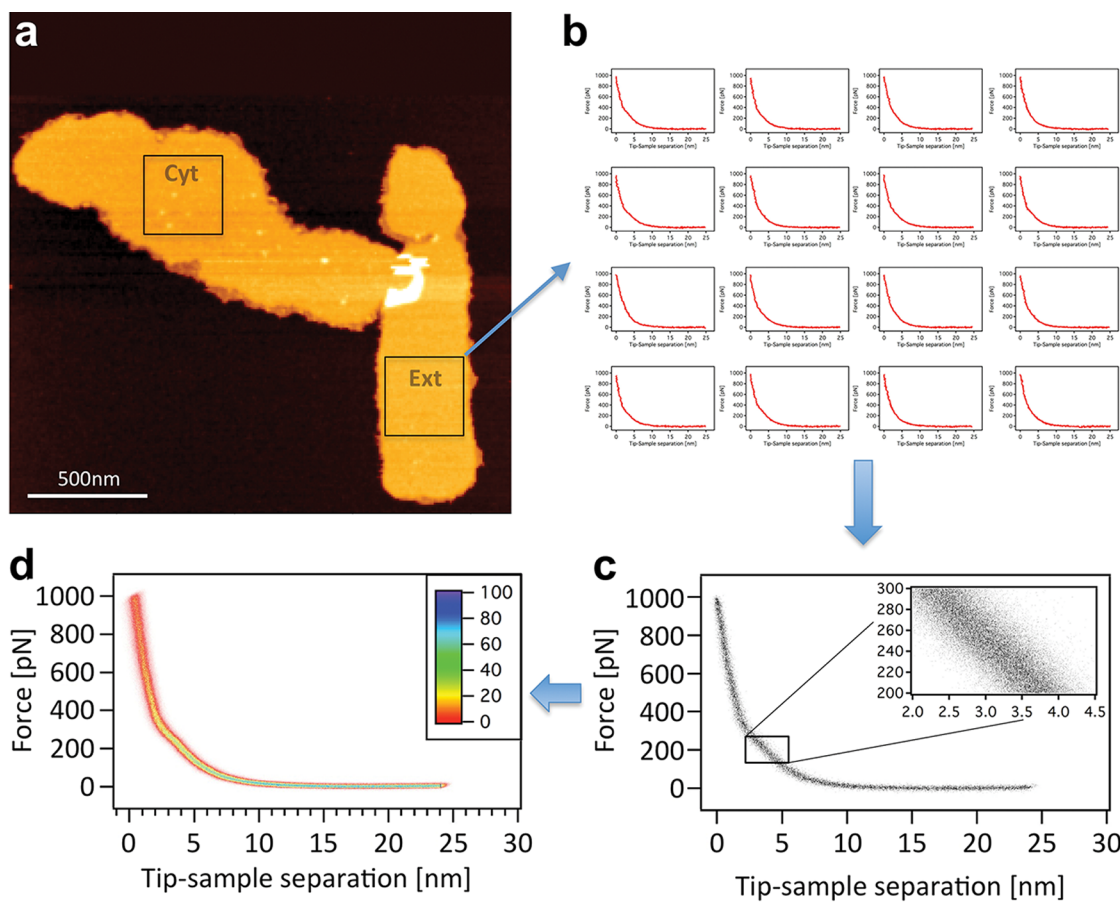


**Figure 1.** AFM topograph and density maps of  $F$ – $D$  curves recorded of purple membrane. (a) FV-AFM topograph showing two purple membranes exposing either their extracellular (ext) or cytoplasmic (cyt) surface.<sup>30</sup> (b)  $F$ – $D$  curves recorded from the marked area on the extracellular surface of purple membrane. (c) Density map of  $\sim 1000$   $F$ – $D$  curves (raw data) that have been superimposed to highlight their common features. All  $F$ – $D$  curves were recorded from the extracellular surface selected in panel a. The inset enlarges the area marked in the density map and shows the distribution of data points of all  $F$ – $D$  curves superimposed. (d) Density map of superimposed  $F$ – $D$  curves displayed in a heat color map. As the density of data points increases the color of the  $F$ – $D$  curve shifts from red to blue. The color inset shows a color map indicating the number of data points superimposed. FV-AFM data was taken in buffer solution (100 mM KCl, pH 7.4, 10 mM Tris-HCl) applying a maximal force of 1000 pN.

At normal circumstances breaking a molecular bond at high loading rate (e.g., high pulling velocity) requires a higher force compared to breaking a bond at lower loading rate (lower pulling velocity).<sup>24,28</sup> For some reasons this effect has hardly been considered when probing the mechanical properties such as strain, shear, strength, or stiffness of complex biomacromolecular systems by FV-AFM. Thus, in the majority of FV-AFM applications the mechanical properties of biomacromolecular systems have been characterized at one loading rate. Moreover, in most cases the loading rate of the AFM tip used to mechanically indent the biomacromolecular sample has not been determined.

In this work we characterize to which extent the mechanical stiffness (e.g., spring constant) of protein membranes depends on the loading rate (e.g., velocity of the AFM tip). As reference sample we have chosen purple membrane as it has been functionally and structurally very well studied and very well characterized by AFM.<sup>8,29–43</sup> Purple membrane consists of 25%

(wt) lipids and 75% (wt) bacteriorhodopsin, which is a light-driven proton pump that spans seven  $\alpha$ -helices across the membrane. We find that the mechanical properties of purple membrane strongly depend on the velocity of the AFM tip. Whereas the extracellular surface of purple membrane is slightly softer compared to the cytoplasmic surface, the mechanical stiffness of both purple membrane surfaces depend on the loading rate of the AFM tip. This stiffness increases roughly linearly with the loading rate. In addition, the electrolyte-dependent electrostatic double layer repulsion between AFM tip and purple membrane works like a cushion that can significantly alter the mechanical stiffness of the purple membrane measured by AFM.<sup>31,44–46</sup> These results suggest that most AFM users must change the way they currently determine the mechanical properties of biological samples. First, it must be considered that the mechanical properties of a biological sample depend on the loading rate.<sup>47</sup> Thus, quantifying the mechanical properties of a biological sample makes little

sense without defining the loading rate at which this property was measured. Moreover, to understand the mechanical properties of a biological system these mechanical properties should be determined over a wide range of loading rates. Second, electrostatic interactions between sample and AFM tip can considerably alter the apparent mechanical properties determined of a biological sample.

## RESULTS AND DISCUSSION

**Analysis of *F–D* Curves Recorded Using FV-AFM.** To characterize purple membrane by FV-AFM the membranes were adsorbed onto freshly cleaved mica.<sup>48</sup> After this, the sample was imaged by FV-AFM at a defined velocity of the AFM tip (Figure 1). The force applied to the AFM tip toward indenting the sample was carefully adjusted to investigate the stability of purple membrane. Purple membranes remained stable applying forces up to 1000 pN and could be repeatedly imaged without any significant structural alteration (Supporting Information, Figure S1). This was in agreement with earlier single-molecule force spectroscopy measurements of purple membrane.<sup>38</sup> When forces of 1200 pN were applied, purple membrane started disassembling (Supporting Information, Figure S1). In contrast, the AFM tip broke through the lipid bilayer surrounding purple membrane at much lower forces (Supporting Information, Figure S2). This highlights the unusual stability of purple membrane, which is dominated by the presence of bacteriorhodopsin.<sup>49,50</sup> It was recently shown, that FV-AFM can also apply very low imaging forces (<40 pN) to contour both purple membrane surfaces in the unperturbed state at subnanometer resolution.<sup>20</sup> However, to probe the mechanical properties of purple membrane we applied forces of up to 1000 pN, which deformed the protein membrane in a reversible manner (Figure 1, Supporting Information, Figure S1). The structural deformation of the protein membrane was revealed from *F–D* curves recorded during FV-AFM imaging. In each *F–D* curve the AFM tip approached the purple membrane surface at a defined constant velocity while recording the tip–sample distance and cantilever deflection. Because for each pixel of the AFM topograph (~2 nm pixel size) one *F–D* curve was recorded we could exclude that we repeatedly probed the same area of the purple membrane (Figure 1b). To allow a statistically significant analysis we superimposed ~1000 *F–D* curves, which were taken from either the cytoplasmic or extracellular purple membrane surface (Figure 1a,b). The superimpositions were displayed as density plots of all (raw) data points recorded from every *F–D* curve (Figure 1c).

Color-coding of the density plots allowed statistically sound evaluation of common features of the *F–D* curves recorded by FV-AFM (Figure 1d). As the density of data points increased the color shifted from white to red to blue. Areas with high density of data points

highlighted a high reproducibility among the *F–D* curves superimposed, whereas areas with lower density of data points showed the variability among the *F–D* curves.

### Characterizing the Electrostatic Contribution to *F–D* Curves.

*F–D* curves recorded on purple membrane, or of any other electrostatically charged biological surface, can detect substantial electrostatic repulsion.<sup>31,45</sup> Depending on the electrolyte concentration of the buffer solution, this electrostatic repulsion can be largely dominated by the electrostatic double layers of counterions that accumulate at the surfaces of the AFM tip and of the purple membrane. As soon as both electrostatic double layers overlap and perturb each other the AFM tip and purple membrane are repelled.<sup>45,51,52</sup> About two decades ago it was shown that this electrostatic double layer repulsion can be directly detected in *F–D* curves.<sup>44,45</sup> Because the electrostatic double layer repulsion is a long-range (several nanometers) interaction that distributes over a large surface area of purple membrane and AFM tip, it hardly contributes to the deformation of the purple membrane surface.<sup>46</sup> However, when sufficiently high force is applied the AFM tip penetrates through the perturbed electrostatic double layer and starts structurally deforming the purple membrane.<sup>46</sup> The force required to overcome the electrostatic repulsion depends on several parameters that are intrinsic to the AFM experiment: The radius and surface charge of the AFM tip, the electrolyte type and concentration, the pH of the buffer solution, and the sidedness of the purple membrane.<sup>31,46,53</sup> However, the force at which the AFM tip physically contacts the purple membrane surface can be estimated from the height of purple membrane recorded in the FV-AFM topograph.<sup>31</sup> Structural characterization by X-ray and electron crystallography shows the thickness of purple membrane to be ~6.2 nm.<sup>35</sup> Imaged by FV-AFM this thickness (height) is reached when applying a force of ~500 pN to the AFM tip. From this we conclude that purple membrane is being compressed as soon as the applied force exceeds 500 pN. To evaluate the electrostatic repulsion contributing to *F–D* curves we recorded FV-AFM topographs of the same purple membrane surfaces in 100 mM KCl and in 300 mM KCl, 40 mM MgCl<sub>2</sub> at pH 7.4 and superimposed ~1000 *F–D* curves for each experimental condition (Figure 2). As expected, *F–D* curves recorded on the extracellular and cytoplasmic surface of purple membrane showed strong dependency on the electrolyte concentration.<sup>31</sup> The higher the electrolyte concentration was, the distance (*i.e.*, thickness) of the electrostatic double layer and the force required to overcome the electrostatic repulsion reduced (Figure 2, black arrows). The *F–D* curves show that at applied forces above ~500 pN the AFM tip overcomes the electrostatic repulsion and structurally deforms the purple membrane (Figure 2, red arrows).

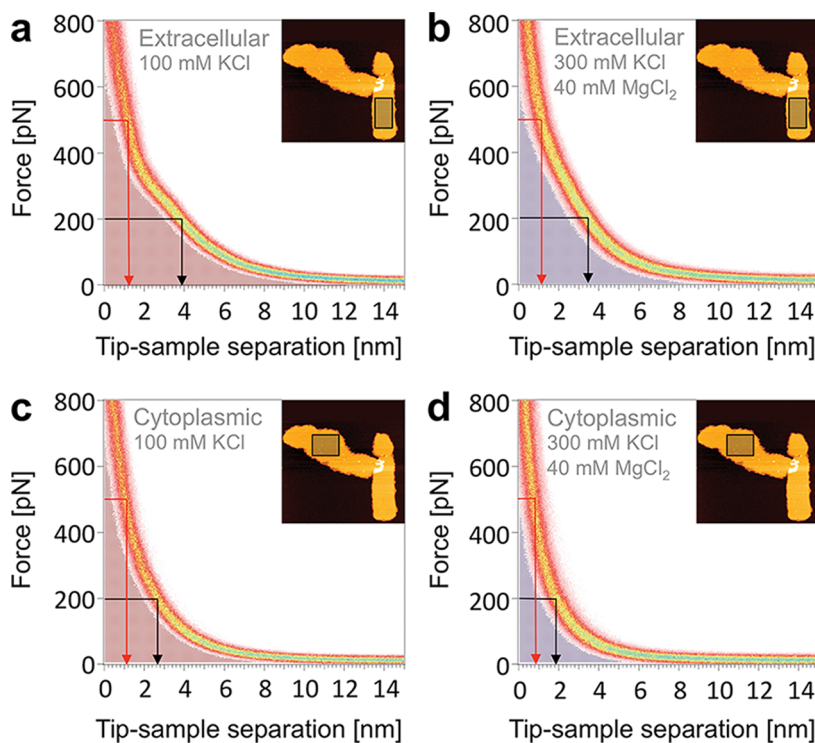


**Figure 2.**  $F$ – $D$  curves recorded on purple membrane depend on electrolyte concentration. Each density plot represents an average  $F$ – $D$  curve from  $\approx 1,000$  superimposed single  $F$ – $D$  curves that were either recorded on the extracellular (a,b) or cytoplasmic (c,d) purple membrane surface. For each density plot an inset outlines the surface area of the purple membrane (Figure 1) from which the  $F$ – $D$  curves were recorded. The slope of the  $F$ – $D$  curves that increases nonlinearly with decreasing tip–sample distance is caused by the electrostatic repulsion between the purple membrane surface and the AFM tip.<sup>31,66</sup> At applied forces  $> 500$  pN (red arrows) the linear slope of the  $F$ – $D$  curve characterizes the structural deformation of purple membrane. Black arrows indicate the tip–sample separation at a force of 200 pN. For the cytoplasmic surface the electrostatic repulsion is lower and, thus, adds less to the tip–sample separation (topographic height) of the purple membrane measured by FV-AFM. The color scale of the density maps is the same as shown in Figure 1.  $F$ – $D$  curves were recorded in buffer solution (pH 7.4, 10 mM Tris-HCl) at the electrolyte indicated.

**Analyzing the Structural Deformation of Both Purple Membrane Surfaces.** After having identified the regions of  $F$ – $D$  curves that stand for the electrostatic repulsion and for the structural deformation of purple membrane we recorded FV-AFM topographs at different tip–sample velocities to see whether electrostatic repulsion and structural deformation depend on the loading rate. From each FV-AFM topograph we extracted and superimposed  $\sim 1000$   $F$ – $D$  curves recorded from the extracellular and the cytoplasmic purple membrane surface (Figure 3, Supporting Information, Figure S3). It became evident that the slope of the  $F$ – $D$  curves depends on the tip–sample velocity. With increasing velocity this slope became steeper indicating that the purple membrane stiffens. This phenomenon was observed for both purple membrane surfaces. At the velocity the  $F$ – $D$  curves were recorded we could rule out that hydrodynamic effects changed the apparent cantilever stiffness.<sup>54</sup>

**Mechanical Properties of Purple Membrane Depend on Loading Rate.** Next, we analyzed the region of the  $F$ – $D$  curve that characterized the structural deformation of the purple membrane (Figure 4a,b). To reveal the mechanical stiffness the linear slope of each density map of  $F$ – $D$  curves recorded at different tip–sample

velocities was fitted in the region between 500 and 1000 pN. From this slope we also calculated the corresponding loading rate (by multiplying the slope with the tip–sample velocity).<sup>24</sup> Plotting the mechanical stiffness recorded at different loading rates revealed an almost linear relationship between stiffness and loading rate (Figure 4c,d). First, we analyzed the stiffness of both purple membrane surfaces in the presence of sufficient electrolyte (300 mM KCl, 40 mM MgCl<sub>2</sub>, pH 7.4, 10 mM Tris-HCl) to screen the electrostatic double layer repulsion (Figure 4c).<sup>31</sup> At the lowest loading rate of 0.6  $\mu$ N/s both purple membrane surfaces showed a mechanical stiffness of  $\sim 0.3$  N/m, which increased almost 10-fold upon approaching the highest loading rate of 100  $\mu$ N/s. In general, the extracellular and cytoplasmic surface showed the same tendency of mechanical stiffness increasing with the loading rate. The mechanical stiffness of the cytoplasmic purple membrane surface was slightly higher ( $\sim 5\%$ ) compared to that determined for the extracellular surface. Such asymmetry of the mechanical properties of the purple membrane was determined earlier by neutron scattering,<sup>50</sup> dynamic mode AFM,<sup>55</sup> and high-resolution FV-AFM.<sup>20</sup> At low loading rates the mechanical stiffness obtained corresponds well to

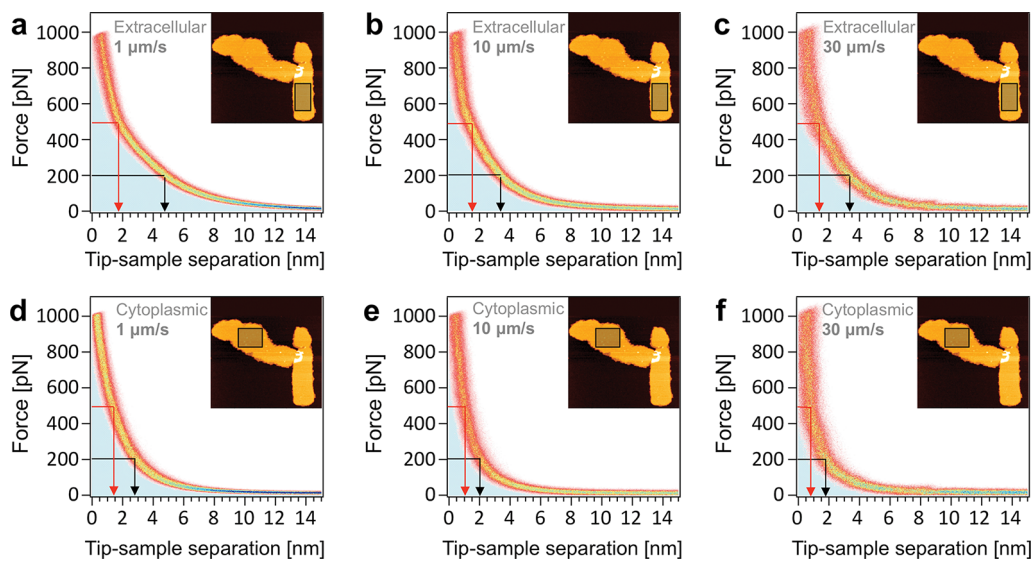


**Figure 3.** Density plots of  $F$ – $D$  curves recorded at different tip–sample velocities on the extracellular (a–c) and cytoplasmic (d–f) purple membrane surface. All  $F$ – $D$  curves change slope with the tip–sample velocity increasing from 1 to  $30\text{ }\mu\text{m/s}$ . The insets outline the surface area of purple membrane from which  $F$ – $D$  curves were taken. Black arrows indicate the tip–sample separation at a force of  $200\text{ pN}$ . Red arrows indicate the region above which the slope of the  $F$ – $D$  curve approaches linearity. Each density plot represents an average  $F$ – $D$  curve from  $\sim 1000$  superimposed  $F$ – $D$  curves either recorded on the extracellular or cytoplasmic purple membrane surface.  $F$ – $D$  curves were recorded in buffer solution ( $300\text{ mM KCl}$ ,  $40\text{ mM MgCl}_2$ , pH 7.4,  $10\text{ mM Tris-HCl}$ ).

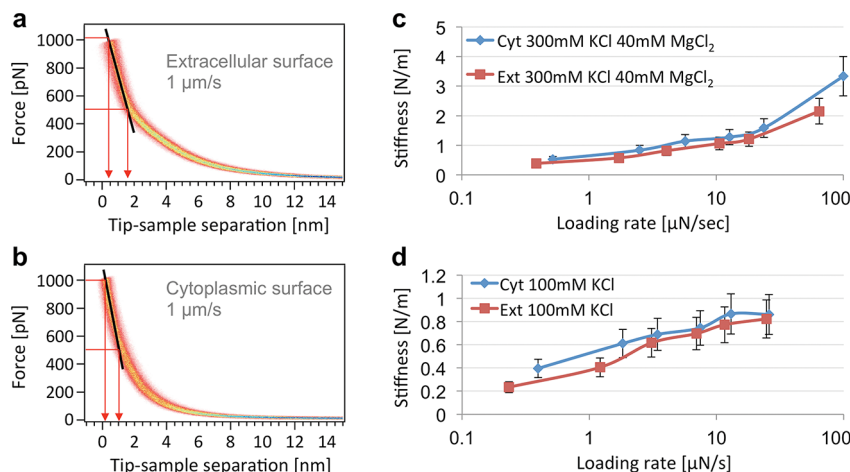


**Figure 4.** The stiffness of purple membrane depends on loading rate and electrolyte. (a,b) Density plots of  $\sim 1000$  superimposed  $F$ – $D$  curves taken at tip–sample velocity of  $1\text{ }\mu\text{m/s}$  on the (a) extracellular and (b) cytoplasmic purple membrane surface in buffer solution ( $300\text{ mM KCl}$ ,  $40\text{ mM MgCl}_2$ , pH 7.4,  $10\text{ mM Tris-HCl}$ ). Red arrows indicate linear regions of  $F$ – $D$  curves that were fitted to reveal the structural stiffness of the mechanically compressed purple membrane. (c) Loading-rate dependent stiffness of the extracellular and cytoplasmic purple membrane surface in the presence of  $300\text{ mM KCl}$ ,  $40\text{ mM MgCl}_2$ , pH 7.4, and  $10\text{ mM Tris-HCl}$ . (d) Loading-rate dependent stiffness of the extracellular and cytoplasmic purple membrane surface in the presence of  $100\text{ mM KCl}$ , pH 7.4, and  $10\text{ mM Tris-HCl}$ .

those previously determined by neutron scattering (0.12–0.55 N/m), dynamic mode AFM, and high-resolution FV-AFM (0.12–0.50 N/m). However, at elevated loading rates the stiffness determined by our dynamic FV-AFM approach differed considerably from published values.

**Electrostatic Repulsion Contributes to Mechanical Properties.** To characterize the influence of electrostatic interactions on the mechanical stiffness determined by FV-AFM we then analyzed  $F$ – $D$  curves recorded on purple membrane in the presence of much less electrolyte

( $100\text{ mM KCl}$ , pH 7.4,  $10\text{ mM Tris-HCl}$ ) (Supporting Information, Figure S3). This analysis was done applying exactly the same procedure introduced for the analysis of the  $F$ – $D$  data recorded at higher electrolyte concentration (Figure 4d). The analysis showed that in the presence of enhanced electrostatic double layer repulsion the mechanical stiffness of purple membrane increased almost linearly with the loading rate. However, the mechanical stiffness of purple membrane in the presence of the enhanced electrostatic double layer repulsion (e.g., at  $100\text{ mM KCl}$ ) was much

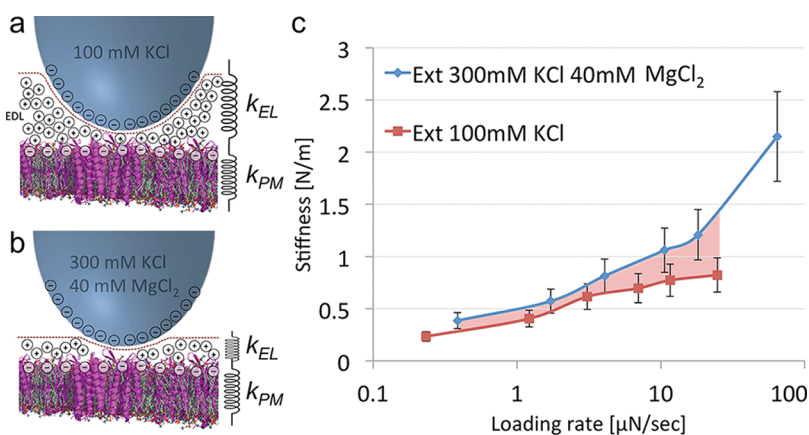


**Figure 5.** Mechanical stiffness of purple membrane shows loading rate-dependent structural and electrostatic contributions. (a) Before contacting the purple membrane the AFM tip has to penetrate the electrostatic double layer. The thickness of this electrostatic double layer depends on the electrolyte concentration of the buffer solution and on the surface charges of AFM tip and purple membrane. Because the electrostatic double layer repels purple membrane and AFM tip it acts like a “mechanical” spring. As soon as the AFM tip physically contacts the biological membrane the membrane starts deforming. This structural deformation acts like a second mechanical spring. The resulting spring constant can be approximated according to eq 1. (b) At enhanced electrolyte concentration the electrostatic double layer becomes thinner. On the basis of these changed properties of the electrostatic double layer, the AFM tip interacts differently with the purple membrane, and consequently the “mechanical” interaction probed by the AFM tip changes. (c) Loading rate dependence of purple membrane stiffness measured at low (100 mM KCl, pH 7.4, 10 mM Tris-HCl) and high (300 mM KCl, 40 mM MgCl<sub>2</sub>, pH 7.4, 10 mM Tris-HCl) electrostatic repulsion (data taken from Figure 4).

lower than the mechanical stiffness recorded in the presence of the weaker electrostatic repulsion (e.g., at 300 mM KCl, 40 mM MgCl<sub>2</sub>). In average the mechanical stiffness of purple membrane in the presence of enhanced electrostatic double layer repulsion was about a factor of 2 lower. This result shows that the electrostatic repulsion between AFM tip and sample influences the mechanical stiffness determined by AFM, even when applying forces that are much higher than that of the electrostatic repulsion.

**Loading-Rate Dependent Biomechanical Properties Show Structural and Electrostatic Origins.** Our results show that the mechanical stiffness of purple membrane is loading-rate dependent and that the electrostatic double layer repulsion between AFM tip and purple membrane can significantly alter the measured stiffness. Thus, two parameters contribute to the mechanical stiffness of purple membrane measured by AFM. At low electrolyte concentration the electrostatic double layers of purple membrane and AFM tip extend over a relatively long distance (several nm) and can be described by a soft cushioning layer (a soft spring) that repels AFM tip and purple membrane.<sup>41,46</sup> To structurally deform the purple membrane the AFM tip must first penetrate the overlapping electrostatic double layers from the AFM tip and purple membrane. As the electrostatic double layer repulsion is of long-range, it distributes over a large surface area of purple membrane and AFM tip. Thus, the local pressure that could deform the purple membrane is quite low and the purple membrane surface is not deformed until the AFM tip gets into physical contact with the purple membrane and applies a sufficiently high, localized pressure.<sup>41,46</sup> This effect is scrutinized in Figure 5a,b. The *F*–*D* curves show

that the slope indicating the electrostatic double layer repulsion (<500 pN) is much flatter than the steep slope characterizing the structural deformation of purple membrane (>500 pN) (Figure 3, Supporting Information, Figure S3). This suggests that purple membrane is mechanically much stiffer compared to the electrostatic double layer repulsion. Therefore, the apparent biomechanical properties of purple membrane as determined by AFM rather reflect a composition of structural and electrostatic contributions. In summary, the overall mechanical stiffness determined of purple membrane  $k_{\text{total}}$  has a structural contribution from the protein membrane  $k_{\text{PM}}$  and an electrostatic contribution from the electrostatic double layer repulsion  $k_{\text{EL}}$ . These contributions of purple membrane and electrostatic repulsion may be described by two sequential springs contributing to the total spring constant:<sup>56</sup>

$$k_{\text{total}} = \frac{k_{\text{PM}} k_{\text{EL}}}{k_{\text{PM}} + k_{\text{EL}}} \quad (1)$$

Thus, the total spring constant measured by the AFM tip will be dominated by the softer spring, which is in this case the electrostatic double layer repulsion. The loading-rate dependence of the mechanical spring constant (stiffness) measured for purple membrane at high and low electrostatic repulsion (Figure 5c) shows that the measured mechanical stiffness (e.g., spring constant) of purple membrane at higher electrolyte concentration (300 mM KCl, 40 mM MgCl<sub>2</sub>) is always higher than that in the presence of lower electrolyte concentration (100 mM KCl). This shows that the mechanical stiffness of purple membrane probed by AFM can be dominated by the much softer electrostatic double layer repulsion.

**Approximating the Spring Constants of Purple Membrane and Electrostatic Repulsion.** In the following we used eq 1 to approach the mechanical spring constant of the electrostatic double layer repulsion at loading rates less than  $1 \mu\text{N}/\text{s}$ . Assuming purple membrane to have a spring constant of  $\sim 0.3 \text{ N/m}$ ,<sup>20,50,55</sup> the spring constant of the electrostatic double layer repulsion approaches  $\sim 0.1 \text{ N/m}$  at  $100 \text{ mM KCl}$ . However, with increasing electrolyte concentration the overall spring constant of the system increases (Figure 5c). This effect is based on the fact that the thickness of the electrostatic double layer and, thus, the electrostatic repulsion between purple membrane and AFM tip reduces with increasing electrolyte concentration (Figures 2, 5a,b).<sup>31,44,46,51</sup> Accordingly, the properties of the electrostatic double layer change significantly. Thus, the overall spring constant of purple membrane increasing with the electrolyte concentration could have several origins: (i) The mechanical properties of purple membrane depend on the electrolyte and stiffen with increasing electrolyte concentration. (ii) The electrostatic double layer becomes thinner with increasing electrolyte concentration and changes “mechanical” properties (*i.e.*, becomes stiffer). (iii) Both cases i and ii play a role.

In our simplified model we have assumed that the mechanical springs detected in our AFM experiments are roughly linear. Certainly, this simplification must be reconsidered and the observed electrolyte-dependent mechanical stiffening of purple membrane may be described by assuming nonlinear springs for particularly the electrostatic repulsion (compare Figures 2 and 3). However, a more accurate description of the effect would require characterizing the contact area between AFM tip, electrostatic double layer, and purple membrane. As this contact area can be hardly defined we approximate the problem by a simplification.

## SUMMARY

The mechanical properties of complex biological samples, such as tissues, cells, membranes, proteins and other biomacromolecular complexes are important to the understanding of various molecular biological, cell biological, tissue engineering, and medical problems.<sup>15,16,57–60</sup> Rheological and AFM experiments on living cells show that the mechanical properties of cells depend on the loading rate.<sup>47,61,62</sup> However, because of the dynamic structural heterogeneity of living cells it is challenging to pinpoint the biomolecular mechanisms and processes leading to a particular cell mechanical property.<sup>63</sup> Nanomechanical properties

are particularly important to understand how biomolecules interact with each other. Thus, the challenge is to quantify the nanomechanical properties of biological systems down to the molecular scale. To characterize these mechanical properties, force-sensing methods such as AFM, optical and magnetic tweezers, and surface force apparatus are applied.<sup>4,5,64</sup> Here we demonstrated that the mechanical property of a biomacromolecular sample depends on the loading rate at which force is applied. In addition, we showed that the mechanical properties determined depend on how the force sensing nanoprobe interacts with the biological sample (*e.g.*, *via* electrostatic repulsion). In AFM the nanoprobe is an AFM tip. However, in a living cell such a probe can be any kind of biomacromolecular system applying, resisting, or sensing mechanical forces. This finding has consequences: One is that determining mechanical properties at the nanoscale requires the characterization of structural and nonstructural (*e.g.*, electrostatic, chemical or other) interactions. A second is that a complete understanding of mechanical properties of biomacromolecular systems requires characterization over a wide range of loading rates. Since interactions of biological systems can range from the ps ( $10^{-12} \text{ s}$ ) to the s range, this means that their nanomechanical properties should be characterized over loading rates ranging several orders of magnitude or at least at rates that are of biological relevance.

Another important issue rises when considering that at the molecular scale biological systems show heterogeneous mechanical properties. Following is the Gedanken experiment: Let us assume that the loading rate dependency of the mechanical properties is intrinsic to a biomacromolecule. The surface of a living cell or cellular membrane is usually composed of a variety of different biomacromolecules and biomacromolecular complexes. If the mechanical properties of individual biomacromolecules and of their complexes shows an intrinsic dependency on the loading rate one can imagine that at certain loading rates the mechanical contrast can change or may even reverse. This example highlights how important it is to characterize the mechanical properties of complex heterogeneous surfaces over a wide range of loading rate. The data also highlight that mechanical properties of biomacromolecular or cellular systems are more complex than those conventionally considered in AFM experiments. Keeping this in mind during future nanomechanical experiments will open new possibilities to understand how mechanical properties of biological systems relate to function.

## METHODS

**Sample Preparation.** Native purple membrane from *H. Salinarum* was prepared for AFM as described.<sup>33,65</sup> Briefly, purple membrane was adsorbed onto freshly cleaved mica in buffer solution

( $150 \text{ mM KCl}$ ,  $10 \text{ mM Tris-HCl}$ , pH 7.6). After 15 min of adsorption, the sample was rinsed with the imaging buffer to remove weakly attached purple membranes.<sup>41</sup> Then, purple membranes adsorbed to the mica were imaged using FV-AFM as

described.<sup>20</sup> Buffers were prepared using nanopure water (18 MΩ/cm) and analytical grade chemicals.

**AFM imaging.** *F–D* curve-based AFM imaging (e.g., FV-AFM) was performed using a closed loop Nanowizard III Ultra AFM (JPK Instruments AG, Berlin, Germany). The AFM used records for every pixel of the topograph one *F–D* curve. To record a *F–D* curve, the AFM tip is moved at linear velocity up and down, which is in contrast to other *F–D* based AFMs that oscillate the AFM tip and therefore move the AFM tip at nonlinear, hardly defined velocity. This nonlinear movement of an oscillating AFM tip makes it difficult to define the applied loading rate. Additionally, in the oscillation mode the AFM tip can be only oscillated at a few selected frequencies. In contrast, at the linear movement the AFM tip travels at (almost) constant velocity that importantly can be freely adjusted. AFM cantilevers used were BioLever mini BL-AC40 (Olympus Corporation, Tokyo, Japan) having a nominal spring constant of 0.1 N/m, a resonance frequency of 100 kHz in air, and a nominal tip apex of 10 nm. All FV-AFM data were taken in buffer solution as specified, at room temperature, and applying imaging amplitudes of 60–70 nm.

**Density maps of *F–D* curves.** Individual *F–D* curves from the FV-AFM topograph were exported as text file using the JPK data processing software (JPK Instruments, AG). Prior to exporting the data each *F–D* curve was treated using the following automatic procedures using the JPK data processing software: The baseline of the *F–D* curve was brought to zero force (offset correction) and the tip–sample separation was calculated from the vertical piezo movement minus the cantilever deflection. Using MatLab (MathWorks Corporation Natick, USA) the FV-AFM topograph was reconstructed from the tip–sample separation (i.e., topographic height) at maximum applied force of the unprocessed approach *F–D* curve. After this, an area of interest was chosen from the FV-AFM topograph, the corresponding *F–D* curves were extracted, aligned according to the first point of the curve, and superimposed. From the superimposed *F–D* curves a density map was created using Igor Pro (WaveMetrics, Portland, USA) and the data points were colored according to their density.

**Stiffness Calculation.** A linear fit was assigned to the linear slope of the density map of superimposed *F–D* curves. This linear region was found to be at forces greater than 500 pN. The stiffness of the purple membrane was calculated from the linear fit according to Hooke's law

$$F = -k\Delta x$$

where  $F$  is the force applied by the tip to the purple membrane,  $\Delta x$  is the tip–sample separation, and  $k$  is the spring constant. The tip sensitivity was calibrated prior to each scan using a density map of ~400 *F–D* curves that were recorded on mica.

**Conflict of Interest:** The authors declare no competing financial interest.

**Acknowledgment.** We thank D. Fotiadis for purple membrane, H. Haschke for technical support, and C. Bippes, J. Helenius, U. Hensen, M. Kammash, and D. Martinez-Martin for critical discussion and reading of the manuscript. EMBO and Swiss National Science Foundation (SNF) supported this work.

**Supporting Information Available:** Purple membrane stability probed by *F–D* curve-based AFM imaging, the characterization of the velocity dependent penetration of the AFM tip through the lipid bilayer, and the velocity dependent force–distance curves recorded on the extracellular and cytoplasmic purple membrane surface at an electrolyte concentration of 100 mM KCl. This material is available free of charge via the Internet at <http://pubs.acs.org>.

## REFERENCES AND NOTES

- Binnig, G.; Quate, C. F.; Gerber, C. Atomic Force Microscope. *Phys. Rev. Lett.* **1986**, *56*, 930–933.
- Heinz, W. F.; Hoh, J. H. Spatially Resolved Force Spectroscopy of Biological Surfaces Using the Atomic Force Microscope. *Trends Biotechnol.* **1999**, *17*, 143–150.
- Gerber, C.; Lang, H. P. How the Doors to the Nanoworld Were Opened. *Nat. Nanotechnol.* **2007**, *1*, 3–5.
- Muller, D. J.; Dufrene, Y. Atomic Force Microscopy as a Multifunctional Molecular Toolbox in Nanobiotechnology. *Nat. Nanotechnol.* **2008**, *3*, 261–269.
- Muller, D. J.; Helenius, J.; Alsteens, D.; Dufrene, Y. F. Force Probing Surfaces of Living Cells to Molecular Resolution. *Nat. Chem. Biol.* **2009**, *5*, 383–390.
- Weisenhorn, A. L.; Khorsandi, M.; Kasas, S.; Gotzos, V.; Butt, H.-J. Deformation and Height Anomaly of Soft Surfaces Studied with an AFM. *Nanotechnology* **1993**, *4*, 106–113.
- Radmacher, M.; Tillman, R. W.; Gaub, H. E. Imaging Viscoelasticity by Force Modulation with the Atomic Force Microscope. *Biophys. J.* **1993**, *64*, 735–742.
- Muller, D. J.; Buldt, G.; Engel, A. Force-Induced Conformational Change of Bacteriorhodopsin. *J. Mol. Biol.* **1995**, *249*, 239–243.
- Rotsch, C.; Jacobson, K.; Radmacher, M. Dimensional and Mechanical Dynamics of Active and Stable Edges in Motile Fibroblasts Investigated by Using Atomic Force Microscopy. *Proc. Natl. Acad. Sci. U.S.A.* **1999**, *96*, 921–926.
- Matzke, R.; Jacobson, K.; Radmacher, M. Direct, High-Resolution Measurement of Furrow Stiffening During Division of Adherent Cells. *Nat. Cell Biol.* **2001**, *3*, 607–610.
- Cross, S. E.; Jin, Y. S.; Rao, J.; Gimzewski, J. K. Nanomechanical Analysis of Cells from Cancer Patients. *Nat. Nanotechnol.* **2007**, *2*, 780–783.
- Francius, G.; Lebeer, S.; Alsteens, D.; Wildling, L.; Gruber, H. J.; Hols, P.; De Keersmaecker, S.; Vanderleyden, J.; Dufrene, Y. F. Detection, Localization, and Conformational Analysis of Single Polysaccharide Molecules on Live Bacteria. *ACS Nano* **2008**, *2*, 1921–1929.
- Sullan, R. M.; Li, J. K.; Zou, S. Direct Correlation of Structures and Nanomechanical Properties of Multicomponent Lipid Bilayers. *Langmuir* **2009**, *25*, 7471–7477.
- Plodinec, M.; Loparic, M.; Monnier, C. A.; Obermann, E. C.; Zanetti-Dallenbach, R.; Oertle, P.; Hyotyla, J. T.; Aebi, U.; Bentires-Alj, M.; Lim, R. Y.; et al. The Nanomechanical Signature of Breast Cancer. *Nat. Nanotechnol.* **2012**, *7*, 757–765.
- Howard, J. *Mechanics of Motor Proteins and the Cytoskeleton*; Sinauer Associates Inc.: Sunderland, MA, 2001.
- Bustamante, C.; Chemla, Y. R.; Forde, N. R.; Izhaky, D. Mechanical Processes in Biochemistry. *Annu. Rev. Biochem.* **2004**, *73*, 705–748.
- Howard, J.; Grill, S. W.; Bois, J. S. Turing's Next Steps: The Mechanochemical Basis of Morphogenesis. *Nat. Rev. Mol. Cell Biol.* **2011**, *12*, 392–398.
- Goehring, N. W.; Grill, S. W. Cell Polarity: Mechanochemical Patterning. *Trends Cell Biol.* **2013**, *23*, 72–80.
- Viani, M. B.; Schäfer, T. E.; Chand, A.; Rief, M.; Gaub, H.; Hansma, P. K. Small Cantilevers for Force Spectroscopy of Single Molecules. *J. Appl. Phys.* **1999**, *86*, 2258–2262.
- Medalsy, I.; Hensen, U.; Muller, D. J. Imaging and Quantifying Chemical and Physical Properties of Native Proteins at Molecular Resolution by Force-Volume AFM. *Angew. Chem., Int. Ed.* **2011**, *50*, 12103–12108.
- Sweers, K. K.; van der Werf, K. O.; Bennink, M. L.; Subramanian, V. Atomic Force Microscopy under Controlled Conditions Reveals Structure of C-Terminal Region of Alpha-Synuclein in Amyloid Fibrils. *ACS Nano* **2012**, *6*, 5952–5960.
- Wegmann, S.; Medalsy, I. D.; Mandelkow, E.; Muller, D. J. The Fuzzy Coat of Pathological Human Tau Fibrils Is a Two-Layered Polyelectrolyte Brush. *Proc. Natl. Acad. Sci. U.S.A.* **2013**, *110*, E313–E321.
- Moy, V. T.; Florin, E.-L.; Gaub, H. E. Intermolecular Forces and Energies between Ligands and Receptors. *Science* **1994**, *266*, 257–259.
- Evans, E.; Ritchie, K. Dynamic Strength of Molecular Adhesion Bonds. *Biophys. J.* **1997**, *72*, 1541–1555.
- Rief, M.; Gautel, M.; Oesterhelt, F.; Fernandez, J. M.; Gaub, H. E. Reversible Unfolding of Individual Titin Immunoglobulin Domains by AFM. *Science* **1997**, *276*, 1109–1112.
- Rief, M.; Gautel, M.; Schemmel, A.; Gaub, H. E. The Mechanical Stability of Immunoglobulin and Fibronectin III

- Domains in the Muscle Protein Titin Measured by Atomic Force Microscopy. *Biophys. J.* **1998**, *75*, 3008–3014.
27. Evans, E. Energy Landscapes of Biomolecular Adhesion and Receptor Anchoring at Interfaces Explored with Dynamic Force Spectroscopy. *Faraday Discuss* **1998**, *111*, 1–16.
28. Evans, E. Probing the Relation between Force Lifetime and Chemistry in Single Molecular Bonds. *Annu. Rev. Biophys. Biomol. Struct.* **2001**, *30*, 105–128.
29. Butt, H.-J.; Prater, C. B.; Hansma, P. K. Imaging Purple Membranes Dry and in Water with the Atomic Force Microscope. *J. Vac. Sci. Technol.* **1991**, *B9*, 1193–1197.
30. Muller, D. J.; Schoenenberger, C. A.; Buldt, G.; Engel, A. Immuno-atomic Force Microscopy of Purple Membrane. *Biophys. J.* **1996**, *70*, 1796–1802.
31. Muller, D. J.; Engel, A. The Height of Biomolecules Measured with the Atomic Force Microscope Depends on Electrostatic Interactions. *Biophys. J.* **1997**, *73*, 1633–1644.
32. Haupts, U.; Tittor, J.; Oesterhelt, D. Closing in on Bacteriorhodopsin: Progress in Understanding the Molecule. *Annu. Rev. Biophys. Biomol. Struct.* **1999**, *28*, 367–399.
33. Muller, D. J.; Sass, H. J.; Muller, S. A.; Buldt, G.; Engel, A. Surface Structures of Native Bacteriorhodopsin Depend on the Molecular Packing Arrangement in the Membrane. *J. Mol. Biol.* **1999**, *285*, 1903–1909.
34. Möller, C.; Allen, M.; Elings, V.; Engel, A.; Müller, D. J. Tapping Mode Atomic Force Microscopy Produces Faithful High-Resolution Images of Protein Surfaces. *Biophys. J.* **1999**, *77*, 1050–1058.
35. Heymann, J. B.; Muller, D. J.; Landau, E. M.; Rosenbusch, J. P.; Pebay-Peyroula, E.; Buldt, G.; Engel, A. Charting the Surfaces of the Purple Membrane. *J. Struct. Biol.* **1999**, *128*, 243–249.
36. Muller, D. J.; Heymann, J. B.; Oesterhelt, F.; Möller, C.; Gaub, H.; Buldt, G.; Engel, A. Atomic Force Microscopy of Native Purple Membrane. *Biochim. Biophys. Acta* **2000**, *1460*, 27–38.
37. Möller, C.; Buldt, G.; Dencher, N. A.; Engel, A.; Müller, D. J. Reversible Loss of Crystallinity on Photobleaching Purple Membrane in the Presence of Hydroxylamine. *J. Mol. Biol.* **2000**, *301*, 869–879.
38. Oesterhelt, F.; Oesterhelt, D.; Pfeiffer, M.; Engel, A.; Gaub, H. E.; Müller, D. J. Unfolding Pathways of Individual Bacteriorhodopsins. *Science* **2000**, *288*, 143–146.
39. Subramanian, S.; Henderson, R. Crystallographic Analysis of Protein Conformational Changes in the Bacteriorhodopsin Photocycle. *Biochim. Biophys. Acta* **2000**, *1460*, 157–165.
40. Lanyi, J. K. Bacteriorhodopsin. *Annu. Rev. Physiol.* **2004**, *66*, 665–688.
41. Müller, D. J.; Engel, A. Atomic Force Microscopy and Spectroscopy of Native Membrane Proteins. *Nat. Protoc.* **2007**, *2*, 2191–2197.
42. Yamashita, H.; Voitchkovsky, K.; Uchihashi, T.; Contera, S. A.; Ryan, J. F.; Ando, T. Dynamics of Bacteriorhodopsin 2D Crystal Observed by High-Speed Atomic Force Microscopy. *J. Struct. Biol.* **2009**, *167*, 153–158.
43. Shibata, M.; Uchihashi, T.; Yamashita, H.; Kandori, H.; Ando, T. Structural Changes in Bacteriorhodopsin in Response to Alternate Illumination Observed by High-Speed Atomic Force Microscopy. *Angew. Chem., Int. Ed. Engl.* **2011**, *50*, 4410–4413.
44. Butt, H. J. Electrostatic Interaction in Atomic Force Microscopy. *Biophys. J.* **1991**, *60*, 777–785.
45. Butt, H. J. Measuring Local Surface Charge Densities in Electrolyte Solutions with a Scanning Force Microscope. *Biophys. J.* **1992**, *63*, 578–582.
46. Müller, D. J.; Fotiadis, D.; Scheuring, S.; Müller, S. A.; Engel, A. Electrostatically Balanced Subnanometer Imaging of Biological Specimens by Atomic Force Microscopy. *Biophys. J.* **1999**, *76*, 1101–1111.
47. Janmey, P. A.; Georges, P. C.; Hvidt, S. Basic Rheology for Biologists. *Methods Cell Biol.* **2007**, *83*, 3–27.
48. Müller, D. J.; Amrein, M.; Engel, A. Adsorption of Biological Molecules to a Solid Support for Scanning Probe Microscopy. *J. Struct. Biol.* **1997**, *119*, 172–188.
49. Tristram-Nagle, S.; Yang, C. P.; Nagle, J. F. Thermodynamic Studies of Purple Membrane. *Biochim. Biophys. Acta* **1986**, *854*, 58–66.
50. Zaccai, G. How Soft Is a Protein? A Protein Dynamics Force Constant Measured by Neutron Scattering. *Science* **2000**, *288*, 1604–1607.
51. Israelachvili, J. *Intermolecular & Surface Forces*; 2nd ed.; Academic Press Limited: London, 1991.
52. Ducker, W. A.; Senden, T. J.; Pashley, R. M. Direct Measurements of Colloidal Forces Using an Atomic Force Microscope. *Nature* **1991**, *353*, 239–241.
53. Butt, H.-J.; Jaschke, M.; Ducker, W. Measuring Surface Forces in Aqueous Solution with the Atomic Force Microscope. *Bioelectrochem. Bioenergy* **1995**, *38*, 191–201.
54. Janovjak, H.; Struckmeier, J.; Müller, D. J. Hydrodynamic Effects in Fast AFM Single-Molecule Force Measurements. *Eur. Biophys. J.* **2005**, *34*, 91–96.
55. Dong, M.; Husale, S.; Sahin, O. Determination of Protein Structural Flexibility by Microsecond Force Spectroscopy. *Nat. Nanotechnol.* **2009**, *4*, 514–517.
56. Uqural, A. C.; Fenster, S. K. *Advanced Strength and Applied Elasticity*, 4th ed.; Prentice Hall: NJ, 2003.
57. Engel, A.; Gaub, H. E. Structure and Mechanics of Membrane Proteins. *Annu. Rev. Biochem.* **2008**, *77*, 127–148.
58. Fletcher, D. A.; Mullins, R. D. Cell Mechanics and the Cytoskeleton. *Nature* **2010**, *463*, 485–492.
59. Haswell, E. S.; Phillips, R.; Rees, D. C. Mechanosensitive Channels: What Can They Do and How Do They Do It? *Structure* **2011**, *19*, 1356–1369.
60. Bukoreshtliev, N. V.; Haase, K.; Pelling, A. E. Mechanical Cues in Cellular Signalling and Communication. *Cell Tiss. Res.* **2012**, *10.1007/s00441-012-1531-4*.
61. Li, Q. S.; Lee, G. Y.; Ong, C. N.; Lim, C. T. AFM Indentation Study of Breast Cancer Cells. *Biochem. Biophys. Res. Commun.* **2008**, *374*, 609–613.
62. Nawaz, S.; Sanchez, P.; Bodensiek, K.; Li, S.; Simons, M.; Schaap, I. A. Cell Visco-elasticity Measured with AFM and Optical Trapping at Sub-Micrometer Deformations. *PLoS One* **2012**, *7*, e45297.
63. Dufrene, Y. F.; Evans, E.; Engel, A.; Helenius, J.; Gaub, H. E.; Müller, D. J. Five Challenges to Bringing Single-Molecule Force Spectroscopy into Living Cells. *Nat. Methods* **2011**, *8*, 123–127.
64. Neuman, K. C.; Nagy, A. Single-Molecule Force Spectroscopy: Optical Tweezers, Magnetic Tweezers, and Atomic Force Microscopy. *Nat. Methods* **2008**, *5*, 491–505.
65. Oesterhelt, D.; Stoeckenius, W. Isolation of the Cell Membrane of *Halobacterium Halobium* and Its Fraction into Red and Purple Membrane. *Methods Enzymol.* **1974**, *31*, 667–678.
66. Butt, H.-J. Electrostatic Interaction in Scanning Probe Microscopy when Imaging in Electrolyte Solutions. *Nanotechnol.* **1992**, *3*, 60–68.